International Journal of Crashworthiness
Publication details, including instructions for authors and subscription information:
http://www.tandfonline.com/loi/tcrs20

Fast strength assessment of mitre gates to ship impact

Loïc Buldgen [a], Hervé Le Sourne [b] & Philippe Rigo [c]
[a] FRIA PhD Student, University of Liège, Dep. ARGENCO, Liège, Belgium
[b] ICAM Nantes Carquefou, France
[c] University of Liège, Dep. ARGENCO, Liège, Belgium
Published online: 05 Jun 2013.

To cite this article: Loïc Buldgen, Hervé Le Sourne & Philippe Rigo (2013): Fast strength assessment of mitre gates to ship impact, International Journal of Crashworthiness, DOI:10.1080/13588265.2013.802146

To link to this article: http://dx.doi.org/10.1080/13588265.2013.802146

International Journal of Crashworthiness, 2013
http://dx.doi.org/10.1080/13588265.2013.802146

Taylor & Francis
Taylor & Francis Group

Fast strength assessment of mitre gates to ship impact

Loïc Buldgen[a*], Hervé Le Sourne[b] and Philippe Rigo[c]

[a]*FRIA PhD Student, University of Liège, Dep. ARGENCO, Liège, Belgium;* [b]*ICAM Nantes Carquefou, France;* [c]*University of Liège, Dep. ARGENCO, Liège, Belgium*

(*Received 9 September 2012; final version received 1 May 2013*)

The present paper is concerned with the design of lock mitre gates submitted to ship impacts. A simplified analytical method is presented to evaluate the resistance of such structures under collision. The basic idea is to assume that the resistance is first provided through a local deforming mode, corresponding to a localised crushing of some impacted structural elements. For consecutive larger deformations, the resistance is then mostly provided through a global deforming mode corresponding to an overall movement of the entire gate. The developments are validated by comparing results obtained numerically to those predicted by the developed analytical approach for mitre gates.

Keywords: mitre gates; ship collision; crashworthiness; super-elements; pre-design calculations

1. Introduction

As reported in [5], it is a fact that lock gates are statistically impacted by vessels several times per year. These minor collisions most of the time result in some slight damages such as loss of watertightness or plating perforation. However, on the entire life of such structures, it is expected that high-speed (>2 m/s) collisions may cause more severe damages, which points out the importance of performing a proper design of gates against vessel impacts.

To do this, it is of course possible to resort to dynamic finite elements analyses. However, doing so may appear to be quite prohibitive at the pre-design stage of gates, because these methods are often time-consuming. This is particularly true when different collision scenarios have to be tested on heavy numerical models. In the present paper, we propose to establish an analytical simplified approach for estimating the global ability of withstanding to collision. The main advantage of such a tool is to quickly provide an approximate idea of the sought resistance. This article will be particularly devoted to the study of mitre gate (Figure 1).

Some results related to the crashworthiness of lock gates have already been published by Le Sourne [8] and Buldgen [3] for plane gates. However, this topic is rarely reported in the literature. On the other hand, many analytical results are available to deal with ship–ship collisions, especially for evaluating the local crushing of the various components constituting the structure of a struck vessel (see for example, references [7–13]). All these developments may be used as a starting point for our analytical approach, but they are not sufficient, because the behaviour of an impacted gate may not directly be assimilated to the one of an impacted vessel. This is mainly due to the fact that a lock gate is much smaller than a ship. When considering a collision on a vessel, it usually assumed that the subsequent deformations are confined in a more or less localised area. For a lock gate, however, as the dimensions of the striking vessel are of the same order of magnitude, a local behaviour may only be expected at the beginning of the penetration. When the indentation is getting larger, the resistance to the impact may no longer be assumed to be only provided by a local deforming region. A global resisting mode is activated, which is not accounted so far in the developments available for treating ship–ship collisions.

2. General presentation of the problem

In this paper, we consider a mitre gate struck by a vessel on one leaf. Due to its particular configuration, it is obvious that the gate will not be able to withstand to a severe collision if the ship is moving upwards. Consequently, we will make the assumption of a ship travelling downwards. In this case, the impact point will be located somewhere on the upstream face.

2.1. Description of the structure

Mitre gates are one of the oldest gate types encountered in lock structures. They are still commonly used today, even though they are mostly devoted to modest locks. On the top view proposed in Figure 2, it can be seen that such gates are made of two leafs, supporting each other through central contact blocks. At their extremities, these leafs are in contact with the lock walls through lateral blocks. All of these connections are only able to transmit normal compressive forces and friction. In other words, neither bending moment nor tensile forces are expected at these locations. It is worth noting that the blocks are positioned on quite

*Corresponding author. Email: L.Buldgen@ulg.ac.be

Figure 1. Mitre gate.

rigid vertical studs making the link between the leaf and its supports.

A simplified overview of one leaf is depicted in Figure 3 (Figure 25). It is made of a plating reinforced by transverse and vertical frames, which constitute the principal stiffening system of the gate. When dealing with collisions, these elements are of prior importance, as they provide the major contribution to the crashworthiness of the struck structure. In addition to these reinforcing frames, transverse and/or vertical stiffeners may sometimes be added in order to prevent the plating to buckle. Their role is mainly to avoid local instabilities under hydrostatic pressure. They do not play an important role in the capacity of the gate to withstand to collision. These elements are not drawn in Figure 3.

It should also be noted that in most cases, a sill is located at the base of the gate. Its primary role is to ensure watertightness and not to provide any supplementary support to structure. However, additional contacts are likely to develop in this region if the gate is collided by a vessel. For this reason, the sill may constitute an indirect restrain to the motion of the gate.

As it can be seen in Figure 3, other particular elements are also required to stabilise the structure. The other support conditions are as follows:

- (1) At the base, the structure is laid on a pivot that allows each leaf to rotate individually when the gate is opening.
- (2) At the top, the structure is hold by one or several ties that are only able to develop tensile forces.

Moreover, each leaf is usually reinforced (at least) by one diagonal diaphragm, linking the upper left corner to the lower right corner of the gate (Figure 3). The role of such component is to reduce the overall bending of the leaf in case of opening. As they do not play a crucial role for the crashworthiness of the structure, such elements will not be considered here.

2.2. *Geometrical properties*

The parameters defining the geometry of the gate are shown in Figure 4. The most important of them is probably the angle α, defining the inclination of each leaf. Usually, for classical mitre gate, α is more or less equal to 20°. The angle β is used to define the declination between the leaf and the lock wall. It is of current practice to consider that $\beta = \alpha$.

To completely characterise the geometry of the struck gate, it is still necessary to give information on the location of the vertical frames along the X axis (Figure 4) and the transverse frames along the Y axis (Figure 3). To each of these elements is associated a given T-shaped cross section that is characterised by the parameters h_w, t_w, h_f, t_f, corresponding to the web height, the web thickness, the flange width and the flange thickness, respectively (Figures 3 and 4).

The geometrical parameters related to the striking ship are plotted in Figure 5. We assume that the shape of the

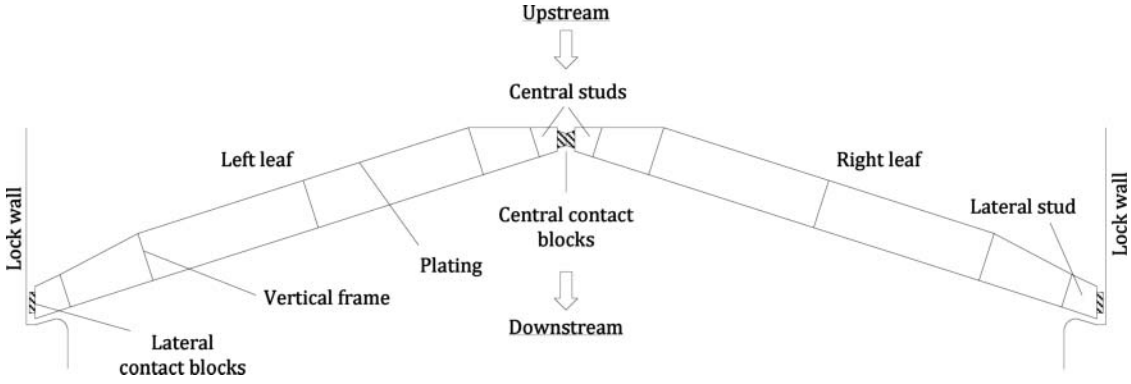

Figure 2. Top view of a mitre gate.

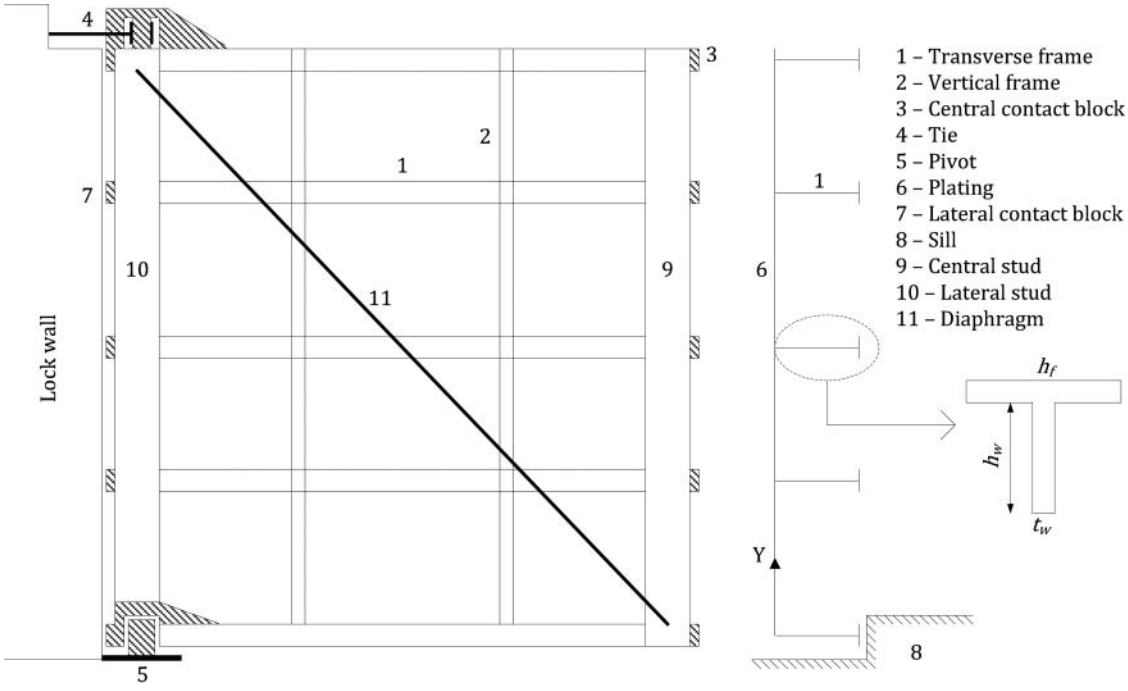

Figure 3. Lateral views of a mitre gate.

uppermost deck may be idealised by a parabola Γ of radii p and q. The distance between the uppermost and lowermost decks is denoted by h_b. The stem and side angles are, respectively, designated by ψ and ϕ. The initial velocity and total mass of the striking ship are denoted by V_0 and M_0, respectively.

Finally, it is still needed to define the relative position between the gate and the ship at the beginning of the collision. As we know, the mathematical expression of the curve Γ (defined as a parabola), it is possible to locate the first contact point P simply by imposing that Γ has to be tangent to the plating of the gate (Figure 6). If we denote by (X, Y, Z) a reference frame located in the plane of a leaf, P is characterised by its abscissa X_P. It is also useful to consider the absolute reference frame (X_0, Y, Z_0), where P is located by its abscissa $X_{0,P}$.

2.3. *Material properties*

During the collision, both the striking ship and the struck structure are likely to deform. However, as this paper is dealing with the resistance of mitre gates, our primary goal

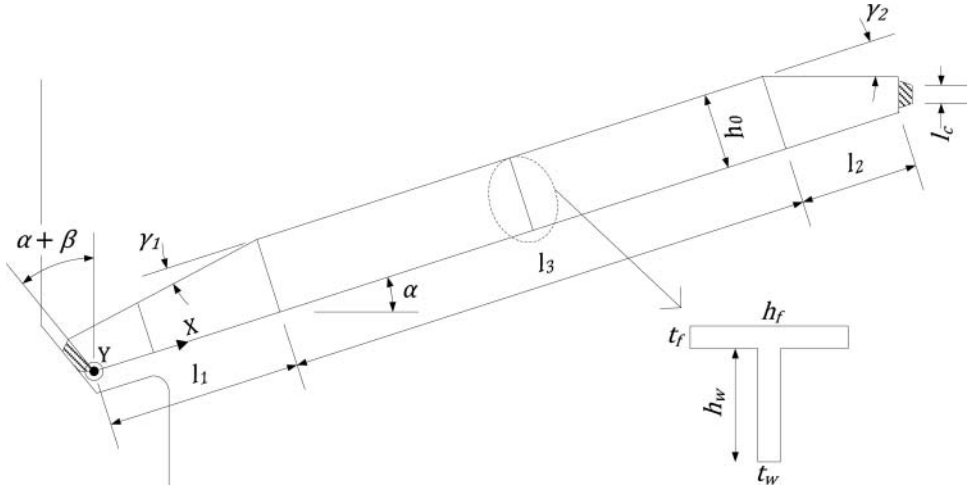

Figure 4. Geometrical parameters defining the gate.

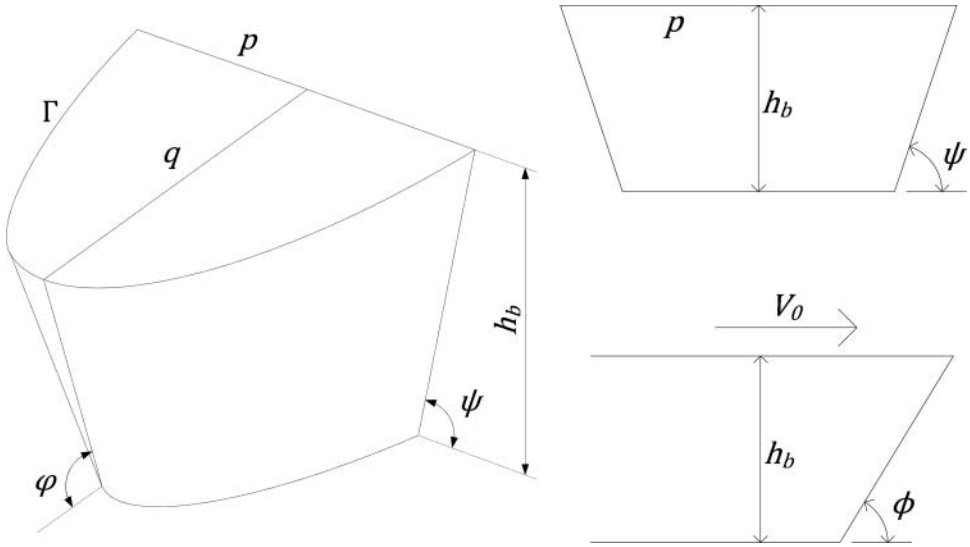

Figure 5. Geometrical parameters defining the striking ship.

is not to estimate the damages caused to the vessel. We will, therefore, admit that the striking ship is made of a perfectly rigid material. As a consequence, the initial kinetic energy $M_0 V_0^2/2$ will have to be entirely dissipated by deformations of the gate. Such an approach is quite conservative, as it implies an overestimation of the collision loads.

The steel constitutive law used for the analytical developments is the simplified one represented in Figure 7. It is defined by the maximal elastic stress σ_0 and Young's modulus E. With such a curve, the non-linear behaviour of steel due to strain hardening is neglected for $\varepsilon > \varepsilon_0$, which is a conservative assumption.

3. Methodology

To develop a simplified procedure leading to a global estimation of the collision resistance $P(\delta)$, we will first suppose that the gate may exhibit two different deforming modes during an impact.

(1) The local deforming mode, associated to a localised indentation of the striking ship. The major part of the structure is not affected by the impact and the penetration of the vessel is mainly allowed by the crushing of some elements in a confined area.

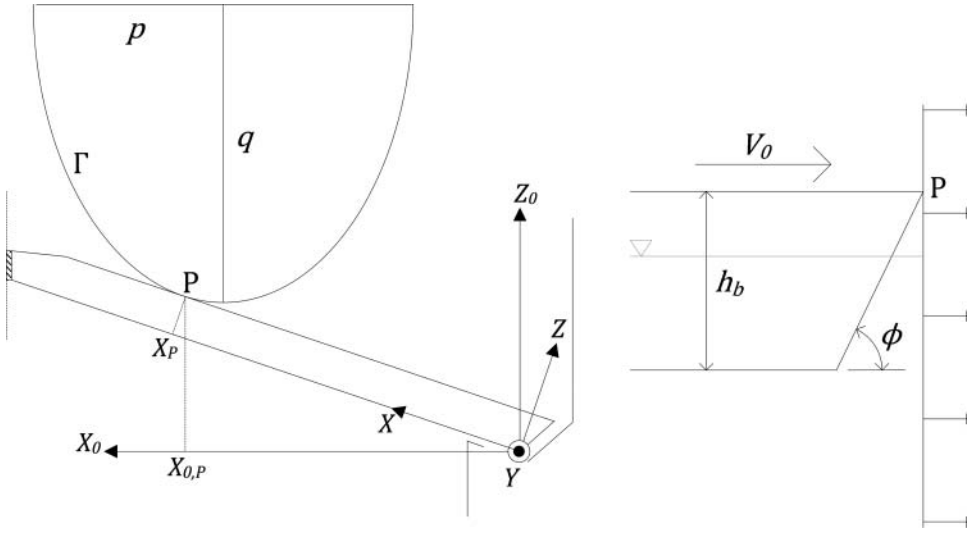

Figure 6. Relative position between the ship and the gate; the first contact point is denoted by P.

Figure 7. Constitutive law of steel used for the analytical developments.

(2) The global deforming mode, associated to an overall deformation of the gate. In this case, the striking vessel keeps moving forward by involving displacements on the entire gate.

These concepts are roughly illustrated in Figure 8, which shows the deformation of a mitre gate collided on its first leaf. As depicted in this figure, some quite localised deformations take place in the region confined around the impact point (see region (1) in Figure 8). This corresponds to the local deforming mode. On the other hand, the top view of the mitre gate also shows that there is an overall bending of the struck structure, which may be directly associated to the global deformation pattern. It is important to distinguish between these two modes, as they influence the behaviour of the gate. This phenomenon has already been detailed by Buldgen [3].

Considering the previous remarks, the determination of P is in fact similar to the evaluation of the resistance developed by the gate in the local (P_{loc}) or in the global (P_{glob}) mode. Our aim is now to develop a simplified approach for estimating P_{loc} and P_{glob}. This is achieved by applying the upper-bound theorem (see Jones [6], for example). However, it is worth bearing in mind that the analytical resistance obtained by applying this theorem is a function of the assumed deformation pattern. As a consequence, this one has to be carefully chosen to get realistic results.

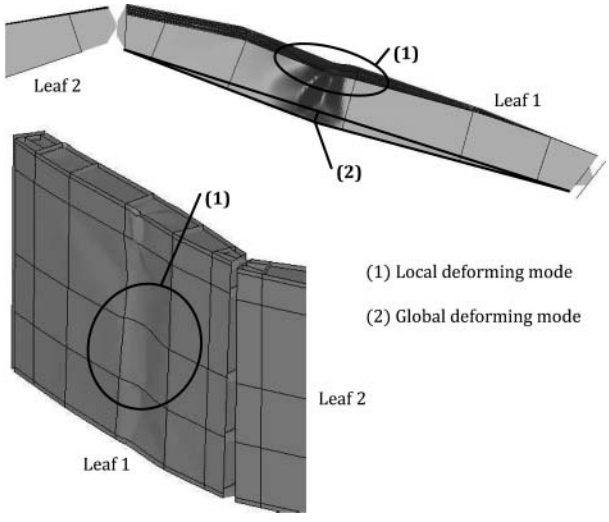

Figure 8. Global and local deforming modes.

4. Local deforming mode

4.1. The super-elements method

In the local deforming mode, we make the hypothesis that the resistance to collision P_{l} is provided through a localised crushing of some components. Assuming a given penetration δ, it is possible to detect the impacted elements which absorb energy by crushing. For example, in Figure 9, it is shown that the current indentation implies not only deformations of the plating, but also crushing of vertical and transverse frames. The displacements remain confined on some structural parts of the structure; there is no overall motion of the gate. These active components of the gate are called 'super-elements'.

The analysis in the local mode is driven by decomposing the entire gate into n_e different super-elements. For each of them, it is possible to derive an analytical formula relating the energy E_i dissipated by the element to the indentation δ of the ship. The total amount of energy locally absorbed is then simply obtained by summation over the Z indentified components. The application of the virtual work principle leads then to the sought value of P_{l},

$$P_{\text{l}}\dot{\delta} = \sum_{i=1}^{n_e} \dot{E}_i, \tag{1}$$

where the dot ($\dot{}$) is used to express a derivative with respect to time. It is worth noting that (1) implies that each element is totally independent from the others. There is no interaction between them, so we implicitly admit that they are decoupled. This strong hypothesis has already been discussed by Buldgen [2], but it is not really questionable as we are also accounting for a global deforming mode, where the coupling between all these super-elements is assessed in a better way.

The goal is now to derive analytical formulations relating E_i and δ for all the components that may be encountered. For modelling the gate, three distinct super-elements are defined hereafter. It should be noted that in a recent paper [2], the super-elements method was extended to analyse oblique collisions between two ships. It is obvious from Figure 10 that the impact of a ship against a mitre gate with an inclination α may be seen as an oblique ship–ship collision occurring at an angle $\pi/2 - \alpha$. Therefore, the super-elements developed in [2] may be directly adopted in the present work. For avoiding any redundancy with [2], the next sections will be quite succinct.

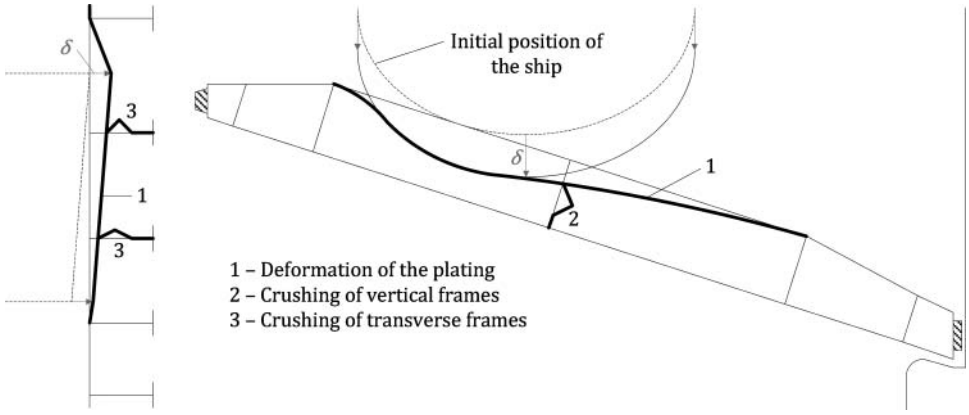

Figure 9. Detection of the impacted super-elements.

4.2. *Super-element 1*

Super-element 1 (SE1) is a plate delimited by two vertical and two transverse frames. It is supposed to be simply supported by transverse and vertical webs. A three-dimensional view of a collision on this super-element is depicted in Figure 11. At the beginning of the impact, the first contact between the ship and SE1 is established at point P (Figure 12). When the ship is moving forward, P is assumed to move to P′ by following a trajectory oriented along Z_0. To define the deformation of the structure, it is convenient to use a displacement field

$W(X, Y)$ that is only oriented along Z, that is, perpendicularly to SE1.

Considering the current position of P′, the initial surface constituting the plate may be divided into four regions (numbered I–IV) in Figure 12. According to the upper-bound theorem, the choice of $W(X, Y)$ is arbitrary, as long as it is kinematically admissible. In the present case, $W(X, Y)$ has to be defined for each of the four regions. For example, considering surface I, we decide to choose

$$W(X, Y) = \left(\frac{X}{a_2 - \delta \sin\alpha}\right)^2 \left(\frac{Y}{b_1}\right)^2 \delta \cos\alpha. \tag{2}$$

Through a similar procedure than the one detailed in [2–13], it is possible to evaluate the contribution of the four regions to the total power associated with SE1. So, for super-element n°i, we have $\dot{E}_i = \dot{E}_{\mathrm{I}} + \dot{E}_{\mathrm{II}} + \dot{E}_{\mathrm{III}} + \dot{E}_{\mathrm{IV}}$, with the following expressions:

$$\dot{E}_{\mathrm{I}} = \frac{8\sigma_0 t_{\mathrm{p}}}{15\sqrt{3}} \left(\frac{1}{(a_2 - \delta \sin\alpha)^2} + \frac{1}{b_1^2}\right) b_1 \times (a_2 + \delta \sin\alpha)\, \delta\dot{\delta} \cos\alpha \tag{3}$$

$$\dot{E}_{\mathrm{II}} = \frac{8\sigma_0 t_{\mathrm{p}}}{15\sqrt{3}} \left(\frac{1}{(a_2 - \delta \sin\alpha)^2} + \frac{1}{b_2^2}\right) b_2 \times (a_2 + \delta \sin\alpha)\delta\dot{\delta} \cos\alpha \tag{4}$$

$$\dot{E}_{\mathrm{III}} = \frac{8\sigma_0 t_{\mathrm{p}}}{15\sqrt{3}} \left(\frac{1}{(a_1 + \delta \sin\alpha)^2} + \frac{1}{b_2^2}\right) b_2 \times (a_1 - \delta \sin\alpha)\delta\dot{\delta} \cos\alpha \tag{5}$$

$$\dot{E}_{\mathrm{IV}} = \frac{8\sigma_0 t_{\mathrm{p}}}{15\sqrt{3}} \left(\frac{1}{(a_1 + \delta \sin\alpha)^2} + \frac{1}{b_1^2}\right) b_1 \times (a_1 - \delta \sin\alpha)\delta\dot{\delta} \cos\alpha. \tag{6}$$

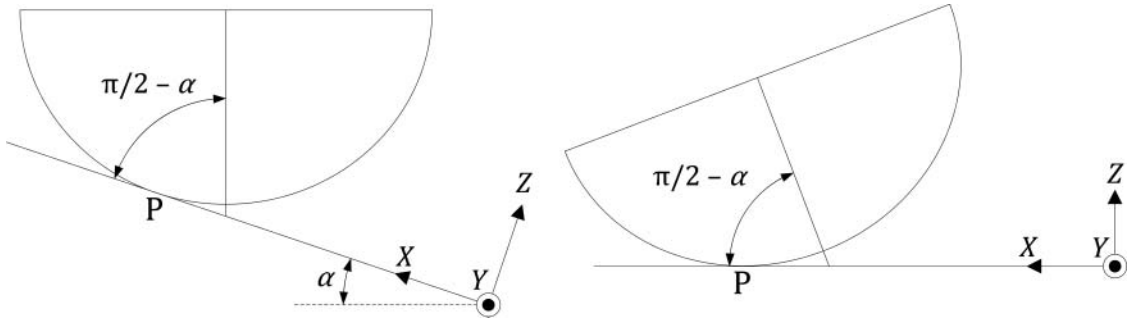

Figure 10. Collision on a mitre gate and oblique collision between two ships.

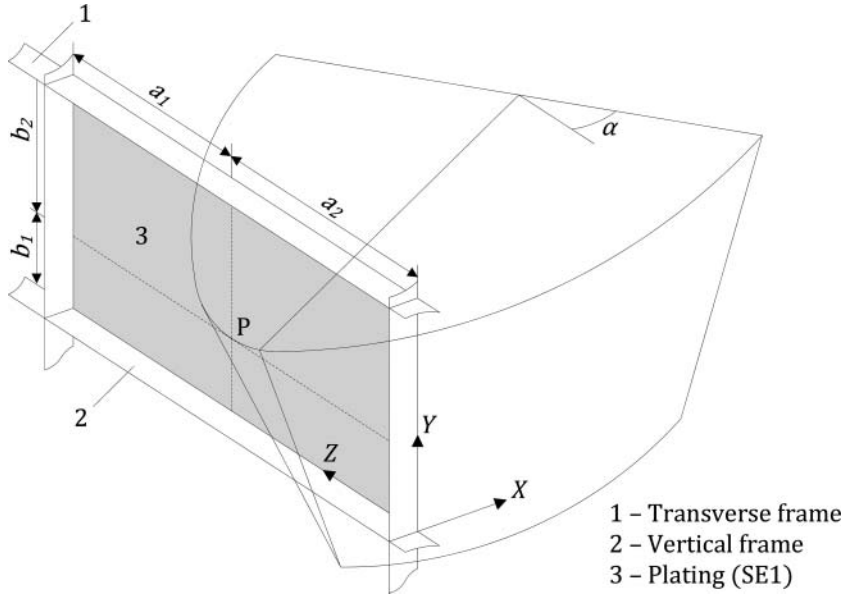

Figure 11. Three-dimensional view of an impact occurring on SE1.

Equations (3)–(6) provide a relation between $\dot{E}_i$ and δ, which was precisely the law sought for evaluating the local resistance offered by SE1.

4.3. Super-element 2

Super-element 2 (SE2) is a transverse or vertical beam with a T cross section. A transverse element SE2 is limited by two vertical frames and vice versa (Figure 14). This element is submitted to an in-plane impact that occurs somewhere between its two support points A and B in Figure 14. If the impact is located on one of these points (i.e. if the collision happens on the intersection between a transverse and a vertical frame), then SE2 has to be treated as an SE3. In the present section, we will only focus on transverse SE2, but the developments are identical for vertical frames. The collision situation is depicted in Figure 13,

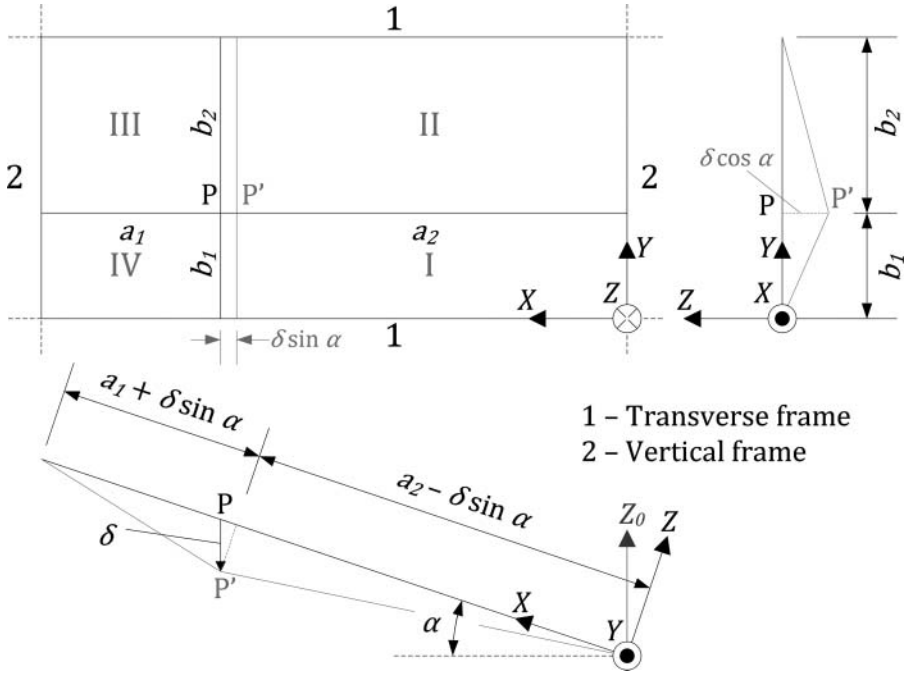

Figure 12. Geometrical parameters and displacement field for super-element 1.

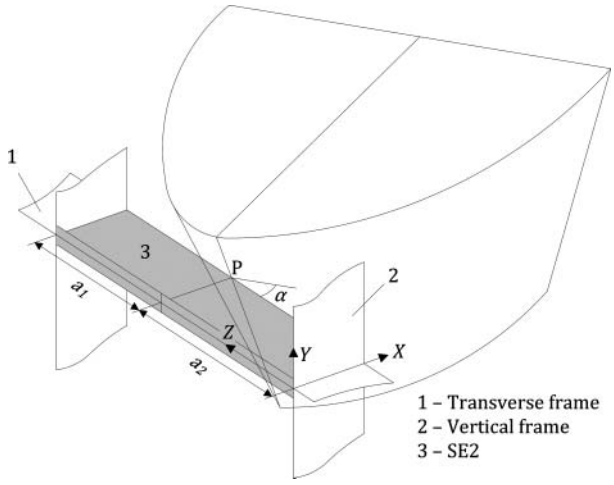

Figure 13. Three-dimensional view of an impact occurring on SE2.

where the super-element is represented by the shaded portions.

The initial contact point P is moving to P′, following the direction given by the axis Z_0. During this motion, we assume that the super-element is folded. The total height of one fold is denoted by $2H$ (Figure 14). So far, H is left as a parameter that will be fixed later. These deformations imply both membrane and bending effects.

(1) To allow the surfaces ADP′, ADC, BDP′ and BDC to rotate, it is necessary to postulate the presence of six plastic hinges in AP′, BP′, AD, BD, AC and BC; otherwise the mechanism would not be kinematically admissible. They are responsible for a bending energy dissipation E_b when a relative rotation between two surfaces occurs.

(2) When the fold is progressively closed, all the above mentioned triangular surfaces are submitted to a tensile field, which results in a membrane energy dissipation E_m.

The total energy dissipated by SE2 n°i during the collision process is simply obtained by summing up the two previous contributions: $E_i = E_b + E_m$.

The folding process has already been extensively study by Wierzbicki [12], Simonsen [9] and [10], Zhang [13] and Buldgen [2], amongst others. Therefore, we will just recall here some results developed in [2].

Concerning bending effects, it is clear that they are directly related to the rotation angle θ. If we assume that the height H is negligible in comparison with a_1 and a_2 (Figure 14), then it can be shown [2] that

$$\dot{E}_b = \frac{\sigma_0 t_w^2}{4}(a_1 + a_2)\,\dot{\theta} = \frac{\sigma_0 t_w^2\,(a_1 + a_2)}{2H\sqrt{1 - \left(1 - \frac{\delta \cos\alpha}{2H}\right)^2}}\dot{\delta}, \tag{7}$$

where t_w is the web thickness of the transverse frame and σ_0 is the flow stress. Other parameters are depicted in Figure 14.

As explained here above, membrane effects are due to an axial straining needed for closing the fold. Under the hypotheses that $H \ll a_1$ and $H \ll a_2$, it can be shown [10] that this extension only implies a displacement field $U(X, Z)$ oriented along the X axis. By neglecting the shearing energy produced by $U(X, Z)$, the only contribution to membrane energy comes from an axial extension of the material fibres parallel to X axis. In this case, we have [2]

$$\dot{E}_m = \frac{\sigma_0 t_w H(a_1+a_2)(\delta(2a_1a_2-(a_1-a_2)\delta\sin\alpha)\cos\alpha+4H(a_1a_2+\delta^2\sin^2\alpha))}{4(a_1+\delta\cos\alpha)^2(a_2-\delta\cos\alpha)^2}\dot{\delta}. \tag{8}$$

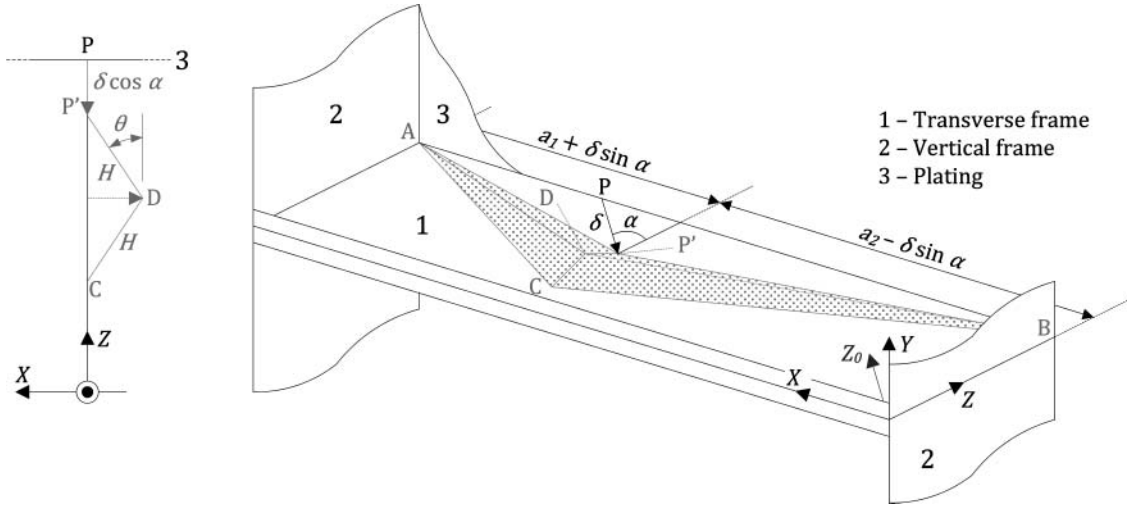

Figure 14. Geometrical parameters and displacements field for super-element 2.

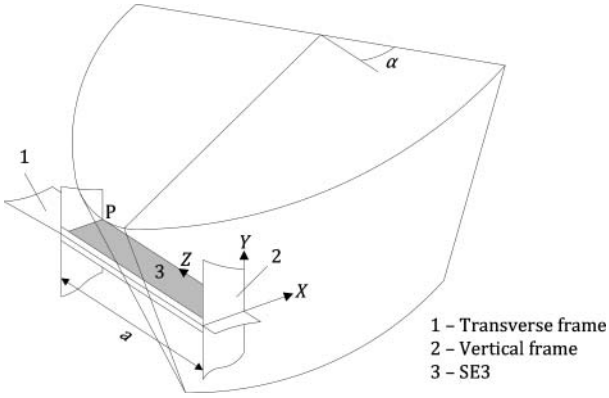

Figure 15. Geometrical parameters and displacement field for super-element 2.

Formulae (7) and (8) may be used to calculate the total rate of energy dissipation $\dot{E}$ for each value of δ, which was precisely the law sought for evaluating the local resistance of SE2. It is still to be noted that the parameter Z_0 is fixed by minimising the mean crushing resistance over one fold. To do so, it can be shown [2] that the following equation is a quite good approximation:

$$H = \sqrt[3]{\pi a_1 a_2 t_w / 12}. \tag{9}$$

4.4. Super-element 3

Super-element 3 (SE3) may be seen as a particular case of the previous section. It is used when the impact is located on the intersection between transverse and vertical frames, as depicted in Figure 15.

In this case, the postulated deformation pattern is the one depicted in Figure 16. The mechanism is made of the triangle BCD folded like a semi SE2, to which is added an additional surface ECDP′ undergoing both folding and compression. The mechanism plotted in Figure 16 is of course also valid for a vertical frame. As a consequence, crushing of an intersection implies an X-shaped or T-shaped deformation pattern, just like the one described by Amdahl [1] or Zhang [13].

When point P moves to P′, it is assumed that the junction PE remains a straight line. Under this assumption, Amdahl [1] showed that the mean value of the power dissipated by the surface ECDP′ over one fold is given by

$$\bar{E}_1 \dot{\delta} = \frac{\sigma_0 t_w}{\sqrt{3}} H \left(\sqrt{k^2 + \frac{1}{4}} \arcsin\left(\frac{1}{\sqrt{4k^2+1}} \right) + k \right) \dot{\delta}, \tag{10}$$

where k is a constant equal to 0.5733. The developments for the triangular surface BCD are quite similar to those performed for SE2, except that the length $a - kH$ is not a function of δ anymore. Following the same procedure as the one applied in [2], the power dissipated by this second part of the mechanism may be written as

$$\dot{E}_2 = \frac{\sigma_0 t_w H}{2(a - kH)} (\delta + 2H) \dot{\delta} + \frac{\sigma_0 t_p^2 (a - kH) \pi}{4H} \dot{\delta}. \tag{11}$$

For each value of δ, the total energy rate associated to an SE3 is simply $\dot{E}_i = \bar{E}_1 \dot{\delta} + \dot{E}_2$, where $\bar{E}_1$ and $\dot{E}_2$ are given by Equations (10) and (11). The optimal value of H is found to be

$$H = \sqrt[3]{\pi t_w a^2} / 12. \tag{12}$$

5. Global deforming mode

5.1. Idealisation of the structure

To develop an analytical procedure for the global deforming mode, we admit that the gate may be seen as a set of beams submitted to a given displacement field. The simplified model of the impacted leaf is shown in Figure 17.

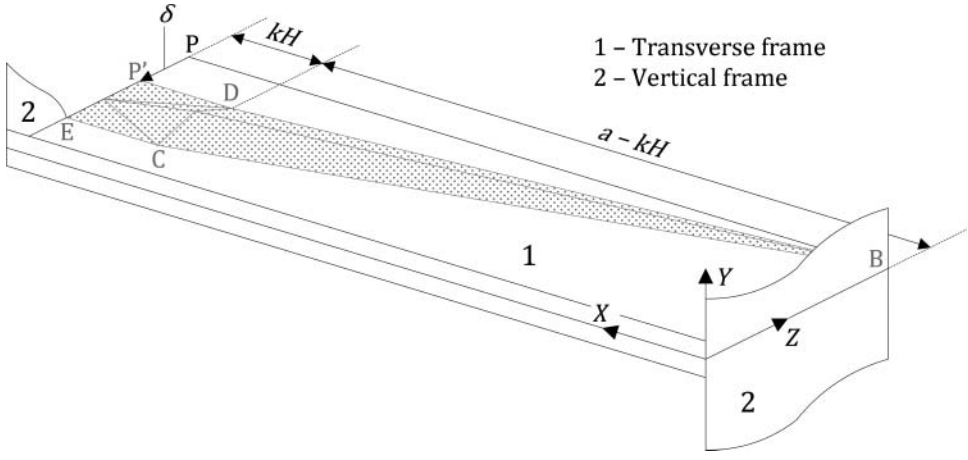

Figure 16. Geometrical parameters and displacement field for super-element 3.

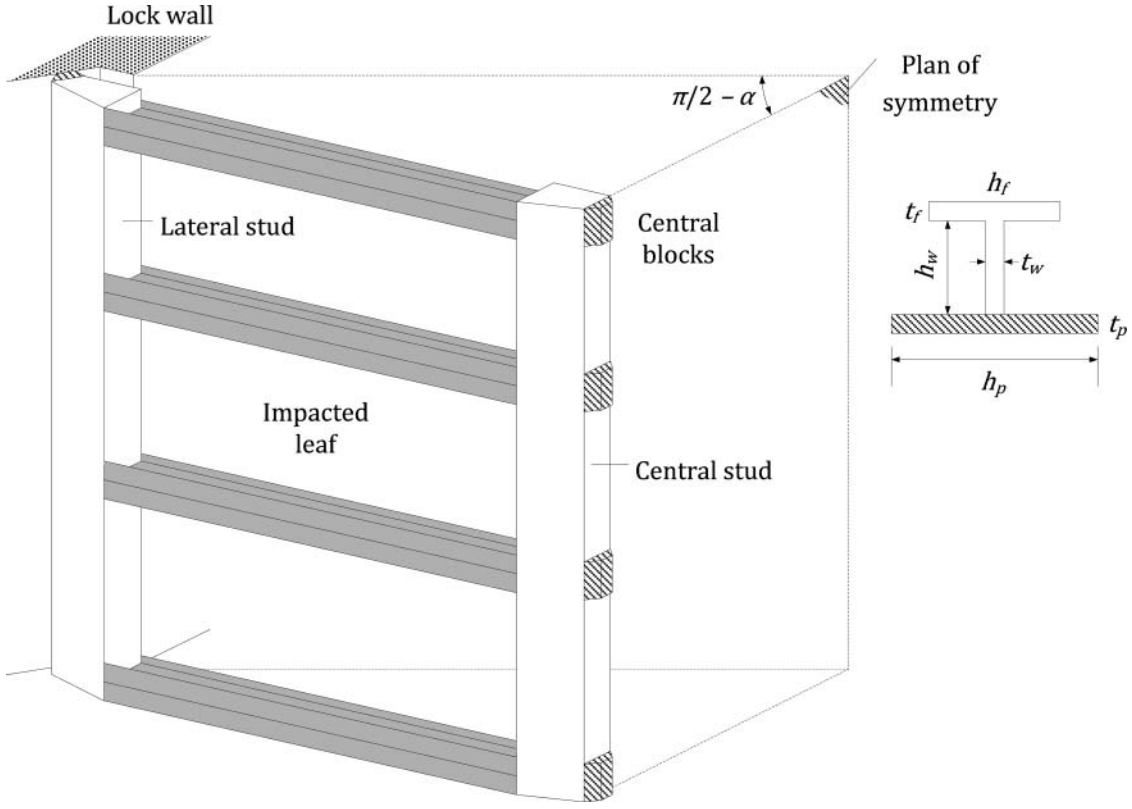

Figure 17. Idealisation of the gate for the global deforming mode.

It is constituted by the transverse frames simply supported by the vertical studs. The connections with the lock wall and the remaining leaf are still insured by the lateral and central blocks. We denote by n_b the total number of beams on each leaf and by Y_i their discrete locations along the vertical Y axis, with $i \in \{1 \dots n_b\}$.

By considering the simplified representation of Figure 17, we implicitly suppose that the vertical frames do not offer an important contribution to the crashworthiness of the structure. In our simplified approach of the global mode, we assume that their role is mainly to provide a connection between the transverse frames, which is required for imposing a given displacement field. By doing so, the mechanical resistance of the vertical girders is neglected, which in some cases may be a strong conservative approach.

Each beam depicted in Figure 17 is made of the cross section of the transverse frames, to which is associated a given collaborating portion of the plating. The resulting cross section is shown on the right part of Figure 17, where h_f, t_f, h_w and t_w have already been presented in Section 2.2. The two other dimensions t_p and h_p are calculated to account for the mechanical resistance offered by the plating. The first parameter t_p is simply equal to the given thickness of the plating. If transverse and/or vertical stiffeners are present for preventing plate buckling, their influence in the collision resistance may be taken into account by smearing them over the plating. This leads to an increased value of t_p. The second parameter h_p may be estimated in accordance with the rules prescribed by EN 1993-1-5 [4] for calculating the effective width of stiffened plates.

5.2. *Elastic resistance of the gate*

At the beginning of the collision, each impacted beam of Figure 17 is first deformed elastically. During this phase, we assume that no motion occurs at the central stud. In other words, point A in Figure 18 is supposed to remain fixed in space. However, this hypothesis is not realistic, as the two leafs are moving back in unison. This is due to friction appearing between the two central contact blocks, as the result that the non-impacted leaf is carried away by the impacted one. Nevertheless, as the elastic phase is quite short, the displacement of point A is much smaller than the indentation δ and it may be neglected. This assumption will be re-examined for the plastic phase.

To apply the upper-bound theorem, the displacements $W(X, Y)$ occurring in the gate during the collision must be postulated. This is roughly illustrated in Figures 18 and 19. Two different frames (X, Y, Z) and (X_0, Y, Z_0) are

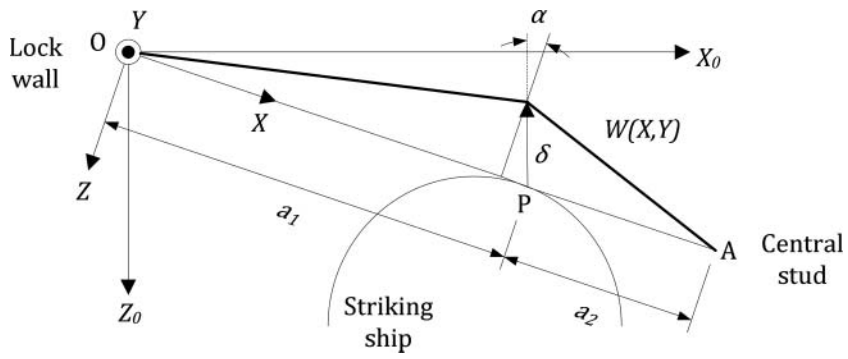

Figure 18. Top view of the displacement field.

introduced (Figure 19). In accordance with Section 2.2, the first contact point P corresponds to a tangential positioning of the ship. The coordinates of P along X and Y are denoted by X_P and Y_P. They allow for the definition of a_1 and a_2, corresponding, respectively, to the lengths of segments OP and AP (Figure 18).

Even if the ship is travelling along Z_0, the field $W(X, Y)$ is defined in the (X, Y, Z) axes. Its amplitude is $\delta \cos\alpha$ (Figure 18) and takes place at $X = a_1 - \delta \sin\alpha$. However, as mentioned earlier, we assume that the elastic phase is quite short, so that the values of δ remain moderate enough for considering a_1 and a_2 instead of $a_1 - \delta \sin\alpha$ and $a_2 + \delta \sin\alpha$.

For the global mode, the displacements $W(X, Y)$ have to be defined on the entire gate. To do so, we admit that $W(X, Y) = f(X)\, g(Y)$. The function $g(Y)$ represents the deflections occurring in a plan π (Figure 19) containing X_P and perpendicular to the leaf. We postulate that

$$\begin{aligned} g(Y) &= \frac{Y}{Y_P}\delta\cos\alpha \quad \text{if} \quad 0 \le Y < Y_P, \\ g(Y) &= \delta\cos\alpha \quad \text{if} \quad Y_P \le Y \le H. \end{aligned} \tag{13}$$

The second term $f(X)$ must respect the support conditions at the lateral $(X = 0)$ and central $(X = a_1 + a_2)$ studs. It is given by

$$f_1(X) = \frac{X}{a_1} \cdot \frac{X^2 + a_1^2 - 2a_1(a_1 + a_2)}{2a_1 a_2} \quad \text{if} \quad 0 \le X < a_1,$$

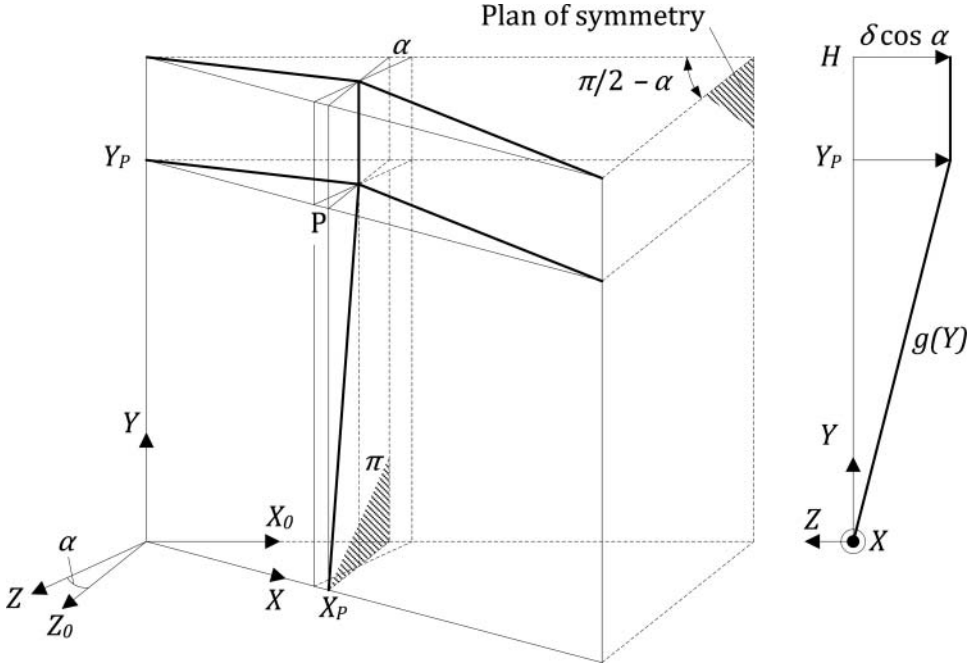

Figure 19. Three-dimensional and plan views of the displacement field.

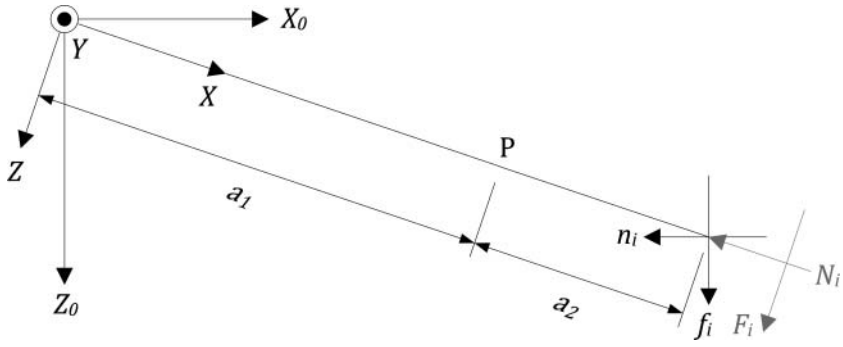

Figure 20. Forces acting at the central contact blocks.

$$f_2(X) = \frac{a_1 + a_2 - X}{a_2} \cdot \frac{X^2 + a_1^2 - 2a_1(a_1 + a_2)}{2a_1 a_2} \quad \text{if} \quad a_1 \le X \le a_1 + a_2. \tag{14}$$

To estimate the internal energy dissipated by the beams during the collision, the internal forces must be evaluated. As mentioned earlier, a beam is bent around its strong axis and follows the previously defined displacement field $W(X, Y)$. However, the gate is also submitted to the action of the hydrostatic pressure, which results into an increased bending of the structure. If the action of the hydrostatic pressure on the frame located at $Y = Y_i$ is denoted by q_i, the total bending moment is given by

$$M_i(X) = \begin{cases} h_b & \text{if} \quad 0 \le X < a_1, \\ X\dfrac{q_i a_1}{2} - EI_i g_i \dfrac{\partial^2 f_2}{\partial X^2} & \text{if} \quad a_1 \le X \le a_1 + a_2. \end{cases} \tag{15}$$

In Equation (15), E is Young's modulus of steel, I_i is the inertia of the cross-section depicted in Figure 17 and $g_i = g(Y_i)$. However, the beam located in $Y = Y_i$ is not only submitted to flexion. Because of the contact between the two leafs, some forces n_i and f_i (Figure 20) are also exchanged at the central contact blocks and have to be transmitted to the lock walls. As n_i and f_i may be decomposed into N_i and F_i along X and Z, the beam has also to be able to withstand to a non-negligible compressive force N_i. The shearing force F_i is then calculated in accordance with the bending moment M_i and it can be shown that

$$\begin{aligned} N_i &= q_i \frac{a_1 + a_2}{2} \cot\alpha + F_i \cot 2\alpha \\ F_i &= q_i \frac{a_1 + a_2}{2} - \frac{\partial M_i}{\partial X}. \end{aligned} \tag{16}$$

The virtual work principle is now applied in order to derive the resisting force P_g opposed by the gate in the global elastic mode. By equating the power developed by the external forces to the internal power dissipated by the gate, we have

$$P_g \dot{\delta} \cos\alpha + \frac{\partial E_w}{\partial \delta}\dot{\delta} = \sum_{i=1}^{n_b} \times \left(\int_0^{a_1+a_2} \frac{N_i}{EA_i}\frac{\partial N_i}{\partial \delta}\dot{\delta} \cdot \mathrm{d}X + \int_0^{a_1+a_2} \frac{M_i}{EI_i}\frac{\partial M_i}{\partial \delta}\dot{\delta} \cdot \mathrm{d}X \right), \tag{17}$$

where A_i is the area of the cross section considered for the beam located in $Y = Y_i$ and E_w is the external work performed by the hydrostatic pressure. Solving Equation (17) finally leads to

$$P_g = \sum_{i=1}^{n_b} \frac{EI_i(a_1 + a_2)g_i}{a_1^2 a_2^2 \cos\alpha} \left(3 + \frac{I_i \cot^2 2\alpha}{4A_i a_2^2}\right) \frac{\partial g_i}{\partial \delta}, \tag{18}$$

where $g(Y)$ is defined by Equation (13). It is worth noting that P_g is assumed to act in plan π (Figure 19), that is, perpendicularly to the plane of the leaf.

5.3. *Plastic resistance of the gate*

For a given value of δ, a plastic hinge is formed on the cross section located in $X = a_1$. The elastic solution exposed previously is then no longer valid and the beam in $Y = Y_i$ is submitted to the laws governing the plastic regime (see Jones [6], for example).

The switch from the elastic to the plastic phase may be detected through a criterion linking M_i and N_i. This interaction curve may be derived by expressing that plasticity has entirely developed on the cross section plotted in Figure 17. Unfortunately, this is quite difficult to do for a non-symmetric section (see Ueda [11] for more details). To simplify the analytical approach, Jones [6] suggested using the interaction criterion developed for rectangular cross

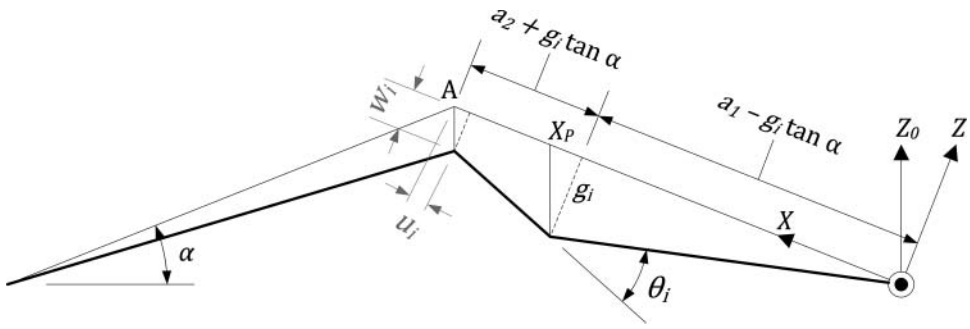

Figure 21. Plastic mechanism assumed for the global bending mode.

sections, given by the following parabolic equation:

$$\frac{M_i}{M_0} + \left(\frac{N_i}{N_0}\right)^2 = 1 \Leftrightarrow M_i = M_0\left(1 - \frac{N_i^2}{N_0^2}\right), \qquad (19)$$

where M_0 and N_0 are, respectively, the plastic bending moment and axial capacity characterising the cross section of the beam located in $Y = Y_i$. By introducing Equations (15) and (16) into Equation (19) and considering $X = a_1$, it is possible to obtain the particular value δ_i of the indentation δ for which the plastic condition (19) is satisfied. Consequently, for $\delta \geq \delta_i$, the mechanism depicted in Figure 21 may be considered. The transverse displacement is still given by $g(Y)$ defined in Equation (13).

The displacement field plotted in Figure 21 is not kinematically acceptable, as it does not respect the continuity of the beam. For this reason, it is necessary to suppose the presence of a plastic hinge. This one is initially located in $X = X_P$, but is forced to move as the striking ship is going forward. For a given value of δ, its current position is given by $X = X_P - g_i \tan\alpha$. This hinge allows for a relative rotation θ_i and leads to a kinematic displacement field.

As mentioned earlier, in the plastic phase, it is also necessary to account for the displacements occurring at the central contact blocks (see point A in Figures 18 and 21). This phenomenon may be quite important because the non-impacted leaf is pushed by the hydrostatic pressure and forced to follow the motions of the collided one. This results into a global backward movement of the entire gate, and consequently, quite large displacements of point A are to be expected. These ones are, respectively, defined by u_i and w_i along the axes X and Z (Figure 21). If we suppose that

$$w_i = \kappa_i g_i \qquad \kappa_i \leq 1, \qquad (20)$$

then w_i is directly proportional to the major transverse displacement g_i, which seems to be a quite reasonable assumption. The parameter κ_i will be fixed later. In addition to Equation (20), we further make the hypothesis that point A is only moving in the direction of Z_0, so that u_i and w_i have to satisfy

$$u_i = w_i \tan\alpha. \qquad (21)$$

The virtual work principle is now written for the plastic configuration by considering the internal and external forces acting on the structure. These ones are depicted in Figure 22, where N_i and F_i are the actions transmitted from one leaf to the other. The bending moment M_i occurs in the plastic hinge and satisfies Equation (19). Moreover, there is an additional relation between M_i and N_i, because the normality condition to the plastic surface has also to be satisfied (see Jones [6] for more details). Considering Equation (19), we have

$$\frac{\mathrm{d}M_i}{\mathrm{d}N_i} = -\frac{\dot{\Delta}_i}{\dot{\theta}_i} \Rightarrow N_i = \frac{N_0^2}{2M_0} \cdot \frac{\partial\Delta_i/\partial g_i}{\partial\theta_i/\partial g_i}, \qquad (22)$$

where $\dot{\theta}_i$ and $\dot{\Delta}_i$ are, respectively, the rotational and axial rates of deformation at the plastic hinge. Assuming that $u_i \ll a_2$, it is easy to see from Figure 21 that

$$\theta_i = \frac{g_i}{a_1 - g_i \tan\alpha} + \frac{g_i(1-\kappa_i)}{a_2 + g_i(1-\kappa_i)\tan\alpha},$$

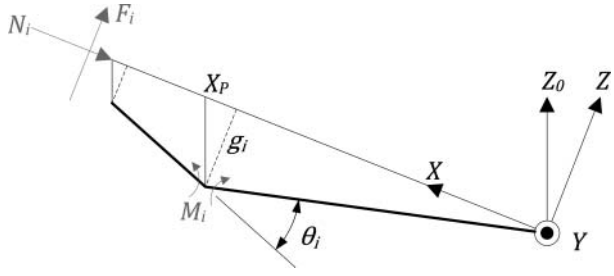

Figure 22. Internal and external forces acting on the beam.

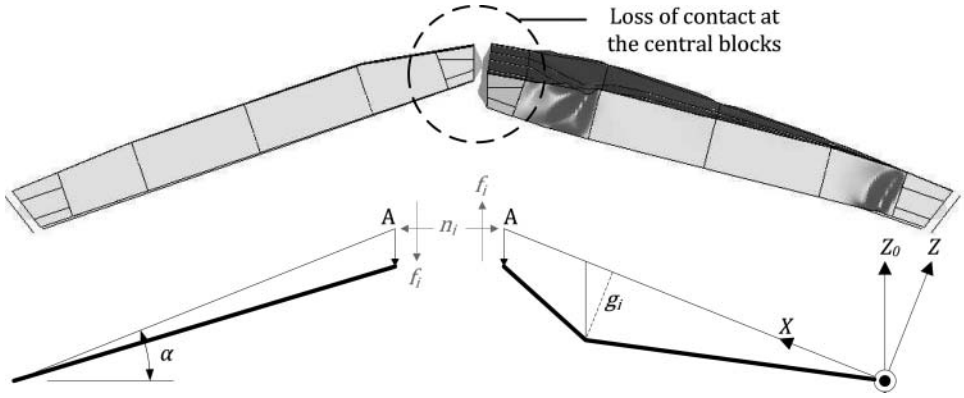

Figure 23. Sliding between the two leafs.

$$\Delta_i = g_i \tan\alpha - \frac{g_i^2(1-\kappa_i)^2}{2(a_2 + g_i(1-\kappa_i)\tan\alpha)} - \frac{g_i^2}{2(a_1 - g_i\tan\alpha)}. \quad (23)$$

If we differentiate Equation (23) with respect to g_i and introduce the results in Equation (22), we get an analytical relation for N_i. Then, with help of Equation (19), it is possible to obtain the bending moment M_i. Finally, considering the equilibrium of forces (Figure 22), the shearing force F_i has to satisfy the following relation:

$$F_i = \frac{M_i - N_i g_i(1-\kappa_i)}{a_2 + g_i(1-\kappa_i)\tan\alpha}. \quad (24)$$

The preceding developments show that it is possible to calculate the internal and external forces acting on the leaf, provided that a suitable value for κ_i is available.

A closed-form expression for κ_i can be found by expressing that the normal force N_i at the beginning of the plastic regime (i.e. when $\delta = \delta_i$) has to be equal to the normal force N_{el} obtained at the end of the elastic phase. The particular value N_{el} is given by Equation (16), with $\delta = \delta_i$,

$$N_{\text{el}} = \left[\frac{3EI_i g_i \cot 2\alpha}{a_1 a_2^2}\right]_{\delta=\delta_i} + \frac{q_i(a_1+a_2)}{2}\cot\alpha. \quad (25)$$

For most of river ship impacts, the elastic phase is quite short and δ_i is very small. Therefore, instead of taking $\delta = \delta_i$ in Equation (22), it is easier to suppose that $\delta_i = 0$ (which is equivalent to have $g_i = 0$). By doing so, it can be shown that Equation (22) leads to

$$N_i = \frac{N_0^2}{2M_0}\left[\frac{\partial\Delta_i/\partial g_i}{\partial\theta_i/\partial g_i}\right]_{g_i=0} = \frac{N_0^2}{2M_0}\cdot\frac{\kappa_i\tan\alpha}{\frac{1-\kappa_i}{a_2}+\frac{1}{a_1}}. \quad (26)$$

Equating (25) and (26) finally leads to the expression of κ_i. This allows for the evaluation of N_i, M_i, F_i, Δ_i, θ_i, u_i and w_i, and it is now possible to evaluate the resistance opposed by the gate during the plastic phase of the global deforming mode. To do so, the virtual work principle is applied by writing that the external power has to be equal to the work rate performed by the internal forces, that is,

$$\begin{aligned} &P_g\dot\delta\cos\alpha + \sum_{i=1}^{n_b}\left(N_i\frac{\partial u_i}{\partial g_i} - F_i\frac{\partial w_i}{\partial g_i}\right)\frac{\partial g_i}{\partial\delta} \\ &= \sum_{i=1}^{n_b}\left(M_i\frac{\partial\theta_i}{\partial g_i} + N_i\frac{\partial\Delta_i}{\partial g_i}\right)\frac{\partial g_i}{\partial\delta}\dot\delta \\ &\Leftrightarrow P_g = \frac{1}{\cos\alpha}\sum_{i=1}^{n_b} \\ &\quad\times\left(M_i\frac{\partial\theta_i}{\partial g_i} + N_i\frac{\partial\Delta_i}{\partial g_i} + F_i\kappa_i - N_i\kappa_i\tan\alpha\right)\frac{\partial g_i}{\partial\delta}. \end{aligned} \quad (27)$$

All the parameters involved in this last expression have been previously derived. Equation (27) is then combined with Equation (18) so as to characterise the complete resistance of the gate during the global mode (i.e. during the elastic and plastic phases).

5.4. *Sliding condition*

As mentioned previously, point A is submitted to a displacement oriented along the Z_0 axis. This also implies a motion of the non-impacted leaf. This movement is imposed through the action of normal and tangent forces (respectively, denoted by n_i and f_i in Figure 23). However, as the indentation is increasing, these forces are not sufficient enough for keeping the contact between each part of the gate. As a consequence, there is a relative sliding

between the central blocks, which finally leads to a loss of contact (Figure 23). This situation may be detected through Coulomb's criteria: if we denote by μ the friction coefficient, then sliding occurs if $f_i > \mu n_i$. The forces n_i and f_i may be directly calculated by considering the previous expressions for N_i and F_i,

$$n_i = N_i \cos\alpha + F_i \sin\alpha \quad f_i = F_i \cos\alpha - N_i \sin\alpha. \tag{28}$$

6. Transition from local-to-global deforming mode

In Sections 4 and 5, we presented closed-form expressions for the local and global resistances, respectively, denoted P_l and P_g. However, this is not sufficient for characterizing completely the resistance P of the gate, because we still have to precise when to use P_l or P_g.

Before describing an overall bending motion, the gate is first submitted to a localised crushing process, the collision resistance P being then equal to P_l. But with increasing values of δ, the vessel forces the structure to describe an overall bending motion. In this second phase, the resistance is principally rising from the global mode and $P = P_g$. Consequently, the method for detecting a switch from local-to-global mode consists to suppose that the structure always tries to offer the smaller resistance to the impact,

$$P(\delta) = \min\left(P_l(\delta); P_g(\delta)\right). \tag{29}$$

The previous approach is valid for lock gates that are quite strongly stiffened, but it can lead to an unrealistic solution if it is not the case. This can be explained by the following reasoning. If the stiffening system (i.e. transverse and vertical frames) is important, the force calculated in the local mode P_l is attempted to increase rapidly. According to Equation (29), the switch from local-to-global mode is therefore supposed to happen for a small value of δ. As a consequence, the damages caused by the local indentation remain moderate, and they do not affect the resistance calculated in the global deforming mode. For such a case, it can be stated that P_l and P_g are decoupled, that is, the damages caused during the local phase have no (or little) influence on the resistance expected in the global one. If this assumption is not verified, then Equation (29) is not valid anymore and other solutions have to be found (see Buldgen [3] for additional details). However, as mitre gate are often reputed to be strongly stiffened, we may consider that Equation (29) applies. The method used for evaluating $P(\delta)$ is illustrated in Figure 24.

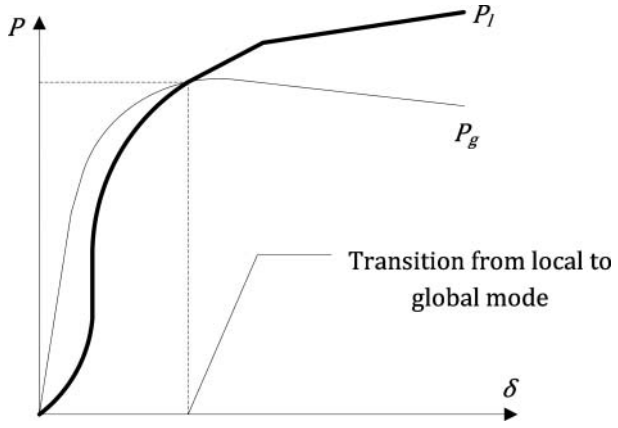

Figure 24. Transition from local-to-global deforming mode.

7. Numerical validation

7.1. Common properties for all the models

To validate the above developments, the analytical approach is now compared with numerical simulations, performed with the finite element software LS-DYNA® 971 (release 4.2.1), for two different gates. A typical mitre gate model used for finite element simulations is shown in Figure 25.

To define the boundary conditions in a realistic way, the lock walls and the sill are also modelled, but considered as rigid. The contact between the gate and the sill is made through the lowermost transverse frame, while the contact with the lock walls is insured by the lateral contact blocks.

At the middle of the gate, the central contact blocks are also modelled. All the above mentioned parts are entirely meshed using Belytschko-Tsai shell elements and a friction coefficient μ of 0.3 is chosen for all defined contacts. The mesh is regular, with a cell size of 5 × 5 cm.

When the gate is pushed against the lock walls, the forces are transmitted through the lateral blocks. However, when the structure tends to separate from the walls, this motion is prohibited by the ties and the pivots. Therefore, these two elements are only acting in tension and are modelled using cable elements that are infinitely stiff in tension but have no stiffness in compression. All the parts of the model are defined with a material representing the behaviour of steel (Figure 26). In the present low-velocity impact model, the strain-rate effect is not taken into account. The used steel characteristics are listed in Table 1.

The stem of the striking ship is assumed to be rigid and is modelled by using the same shell elements as for the gate. The dimensions of the striking ship, listed in Table 2, are defined in accordance with Figure 5.

Table 1. Parameters defining the material law of steel.

Density (kg/m^3)	ρ	7850
Poisson's ratio	ν	0.33
Yield stress (MPa)	σ_0	240
Young's modulus (MPa)	E	210, 000
Tangent modulus (MPa)	E_T	1018

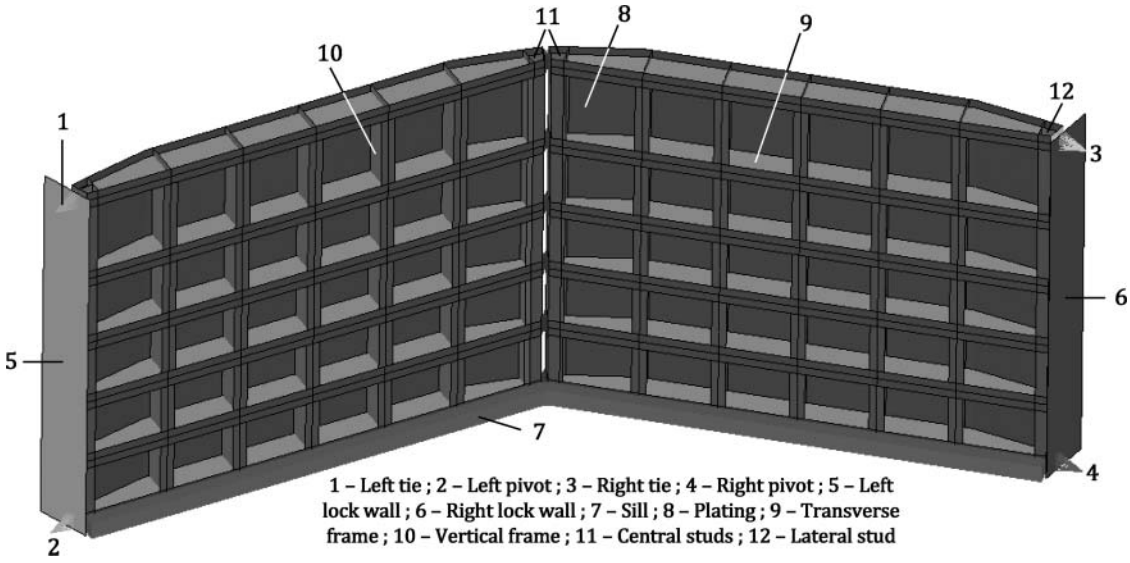

Figure 25. Typical finite mitre gate model (the refined mesh is not shown here).

7.2. *Gate model 1*

The geometrical properties of gate 1, listed in Table 3, are defined in accordance with the notations introduced in Figure 4 and in the other sections of the text. The vertical positions Y_i of the transverse frames are given by a vector, so as to have $Y_1 = 0$ till $Y_6 = 6.5$ m.

The numerical and analytical curves showing the crushing resistance $P(\delta)$ are plotted in Figure 27 and the equivalent von Mises stresses given by LS-DYNA are represented in Figure 28. The numerical simulation was performed until sliding occurs between the two leafs (Figure 23).

It is shown by Figure 27 that the solution obtained by the simplified procedure exposed in this paper provides a rather satisfactory estimation of the numerical solution, but some discrepancy may be observed. This is mainly due to the fact that the impact is located near the intersection between the uppermost transverse frame and a vertical one. Therefore, according to Figures 13 and 14, a_2 is quite small, and consequently, the assumption $H \ll a_2$ of Section 4.3 is no longer verified for SE2 (in the present case, $a_2 \approx 0.3$ m and $H \approx 0.15$ m). The deformations in the uppermost horizontal frame are therefore quite important, leading to high values of the local resistance. This forces the transition to the global resisting mode to be activated for a quite small value of penetration ($\delta \approx 0.07$ m in Figure 27), which explains why the analytical curve underestimates the results provided by LS-DYNA for $\delta > 0.07$ m in Figure 27. However, this situation seems to be acceptable as it leads to somewhat conservative results.

Table 2. Numerical data for the striking vessel.

p	q	φ	ψ	h_b	M_0	V_0
6 m	8 m	84°	84°	5 m	4000 t	2 m/s

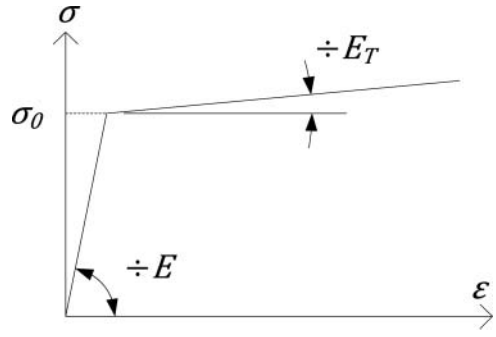

Figure 26. Stress–strain relation of steel.

7.3. *Gate model 2*

The second considered gate is much larger than the previous one. The stiffening system has been reinforced by increasing the dimensions of the transverse and vertical frames. The main characteristics are listed in Table 4. For this simulation, the first contact point P is defined by $X_P = 8.2$ m and $Y_P = 7.15$ m (Figure 5).

The numerical and analytical curves of $P(\delta)$ are plotted in Figure 29 and show that the accordance between both of them is quite satisfactory. The analytical curve remains conservative. The simulation was stopped when sliding between the two leafs occurred, which is the reason why the resistance abruptly decreases around $\delta = 0.9$ m.

7.4. *Sensitivity analysis*

Some additional simulations were also performed in order to check the validity of the simplified approach in various

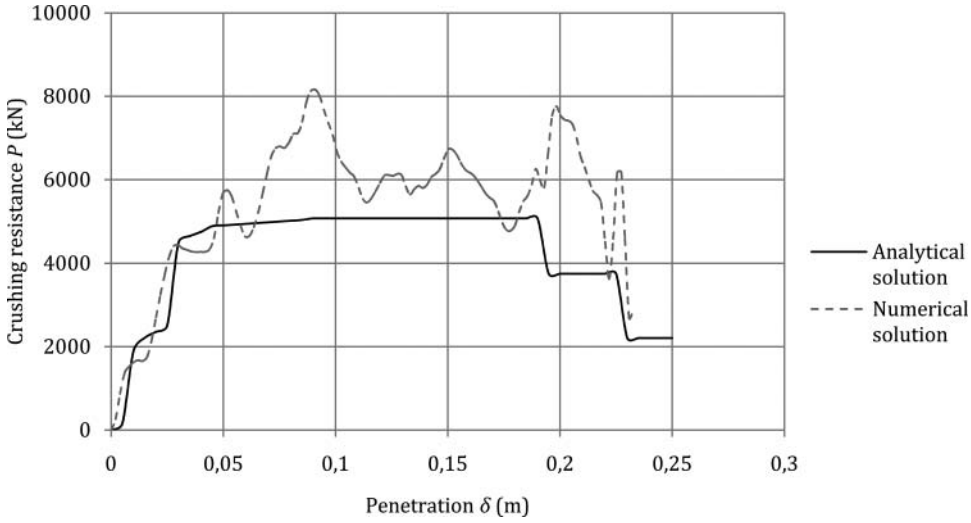

Figure 27. Numerical and analytical resistance curves for gate model 1.

other cases. They are all based on the second gate model, but some parameters are varied:

- Gate model 2.1: the impact point location is changed. Y_P is still equal to 7.15 m, but this time $X_P = 12.6$ m. With this configuration, the collision occurs near the central stud. The results, presented in Figure 30, show that sliding occurs around $\delta = 0.7$ m, so it does not really matter if the analytical curve is not conservative for $\delta \geq 0.7$ m.
- Gate model 2.2: the importance of the stiffening system is reduced. To do so, in comparison with Table 4, the thickness of the plating and of the transverse frames are, respectively, reduced to $t_p = 0.015$ m and $t_w = 0.012$ m. The impact is kept at $X_P = 8.2$ m and $Y_P = 7.15$ m. The curve obtained in this case is plotted in Figure 31, and shows a rather good accordance with the numerical results obtained using LS-DYNA. The analytical approach is once again quite conservative.

Table 3. Geometrical properties for gate 1.

General data		Transverse frames			Vertical frames		
l_i (m)	1.41	Flange thickness (m)	t_f	0.06	Flange thickness (m)	t_f	0.04
l_2 (m)	1.41	Flange width (m)	h_f	0.3	Flange width (m)	h_f	0.25
l_3 (m)	5.58	Web thickness (m)	t_w	0.03	Web thickness (m)	t_w	0.024
α	18°	Web height (m)	h_w	0.6	Web height (m)	h_w	0.61
β	18°	Plating thickness (m)	t_p	0.02			
γ_1	12°	Total number	n_b	6			
γ_2	12°	Vertical position (m)	Y_i	{0 1.2 2.4 3.6 4.9 6.5}			

Note: For this simulation, the first contact point P is located at the middle of the leaf (i.e. $X_P = 4$ m according to the notations of Figure 5). The vertical position of P is given by $Y_P = 6.3$ m, so the collision occurs in the upper part of the gate (the total height of the gate is $H_g = Y_6 = 6.5$ m).

Table 4. Geometrical properties for gate 2.

General data		Transverse frames			Vertical frames		
l_1 (m)	3.35	Flange thickness (m)	t_f	0.012	Flange thickness (m)	t_f	0.012
l_2 (m)	3.15	Flange width (m)	h_f	0.4	Flange width (m)	h_f	0.3
l_3 (m)	7	Web thickness (m)	t_w	0.016	Web thickness (m)	t_w	0.012
α	19°	Web height (m)	h_w	1.5	Web height (m)	h_w	1.5
β	19°	Plating thickness (m)	t_p	0.022			
γ_1	6°	Total number	n_b	5			
γ_2	10°	Vertical position (m)	Y_i	{0 2.53 5.23 9.06 10.3}			

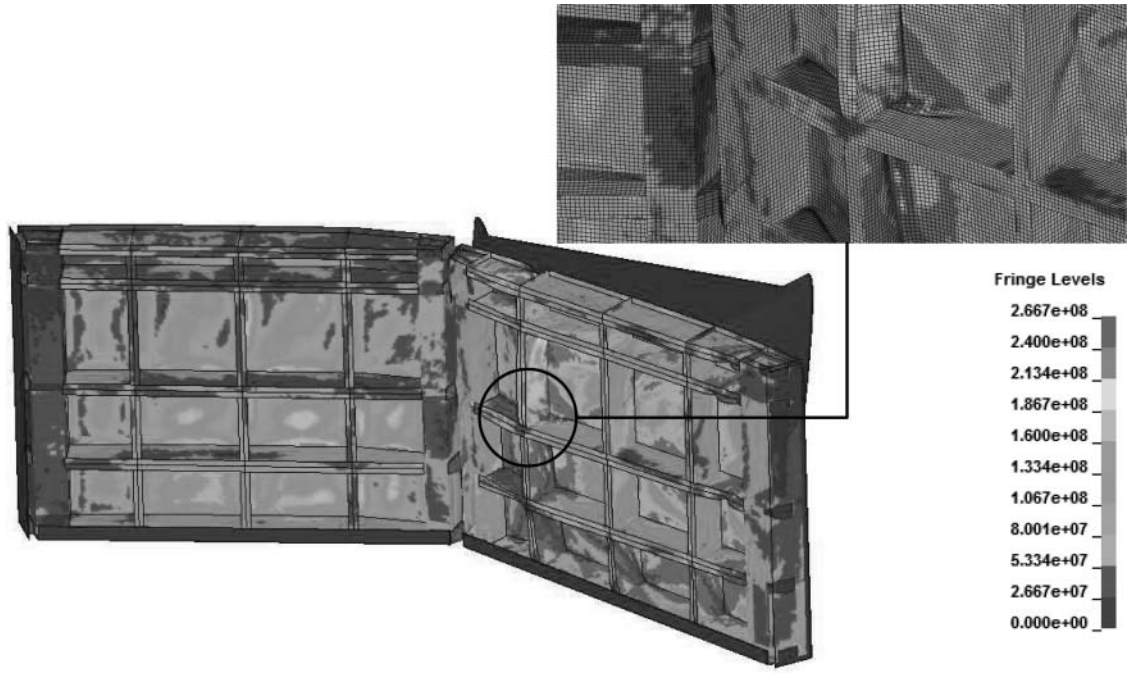

Figure 28. von Mises stresses (MPa) in the deformed configuration of the gate according to LS-DYNA.

- Gate model 2.3: the importance of the stiffening system is the time increased by modifying the thickness of the transverse frames to have $t_w = 0.02$ m and $t_f = 0.02$ m. The impact is still located at $X_P = 8.2$ m and $Y_P = 7.15$ m. This leads to the curves depicted in Figure 32. Conservative results are provided by the analytical procedure at the beginning of the penetration, but it is not always the case when $\delta > 0.2$ m where the crushing resistance tends to be overestimated in comparison with numerical results. This is partially due to the hypothesis that the local and global modes are strictly separated. It is shown by the numerical simulations that the ship is sometimes moving forward through an increased local indentation and sometimes through an increased overall bending of the gate. This phenomenon is not taken

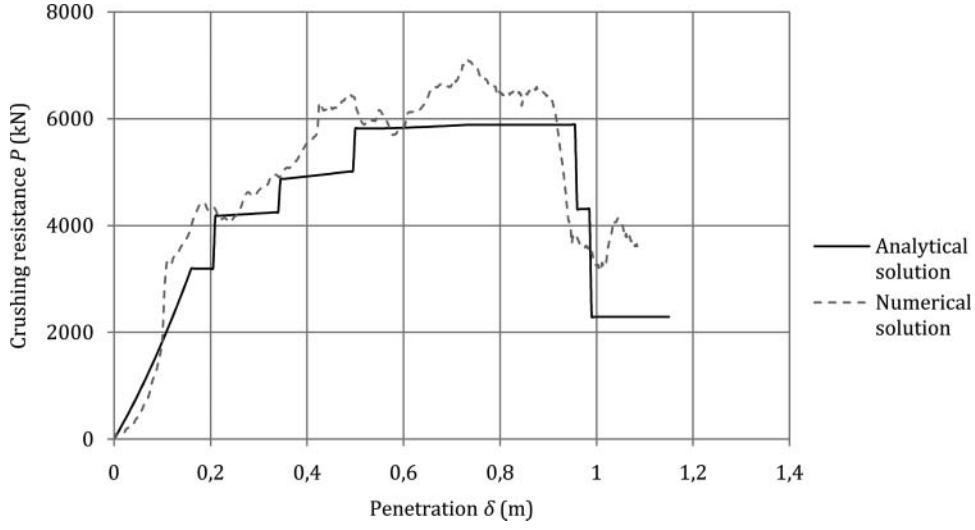

Figure 29. Numerical and analytical resistance curves for gate model 2.

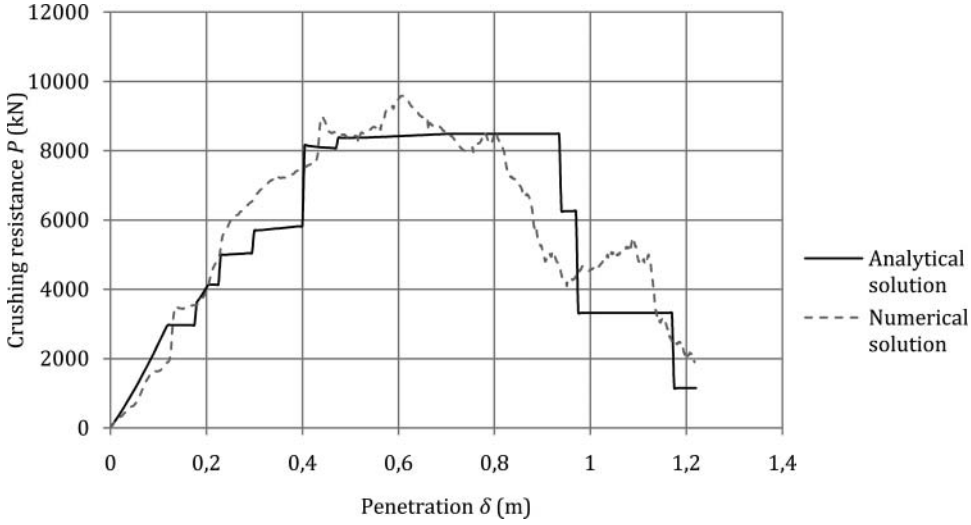

Figure 30. Numerical and analytical resistance curves for gate model 2.1.

into account in the present simplified analytical approach. However, the discrepancy between the two curves remains acceptable.

- Gate model 2.4: the influence of the vertical frames is now investigated. In the present approach, it is assumed that their role is only to transmit the displacement field to the transverse frames. However, this hypothesis may not be valid anymore if the vertical frames are too weak to force the collaboration between the transverse ones. Therefore, the properties of the vertical girders are reduced to the following values: $t_w = 0.01$ m, $t_f = 0.01$ m and $h_w = 1.2$ m. The impact is kept at $X_P = 8.2$ m and $Y_P = 7.15$ m. The corresponding results are plotted in Figure 33 with a quite good agreement.

It is shown by the sensitivity analysis performed in this section that the simplified procedure leads to quite acceptable curves in comparison with those obtained numerically with LS-DYNA. Most of the time, the approach appears to be conservative, which is an important point regarding the future use of the method, that is, at a pre-design stage of the gate. The hypothesis made on the vertical frames is also confirmed by this study: even if they are weakened, they still continue to play their role by transmitting the displacements from one transverse frame to the others.

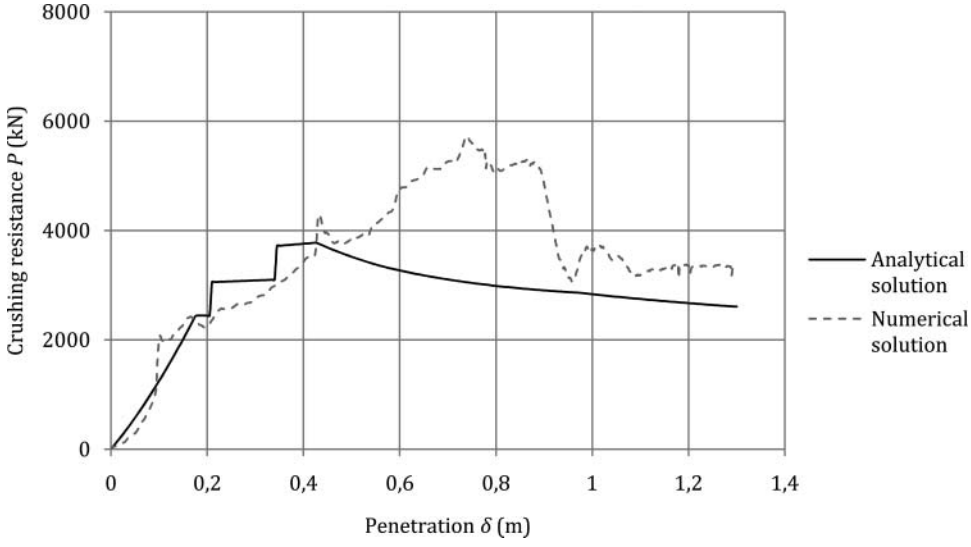

Figure 31. Numerical and analytical resistance curves for gate model 2.2.

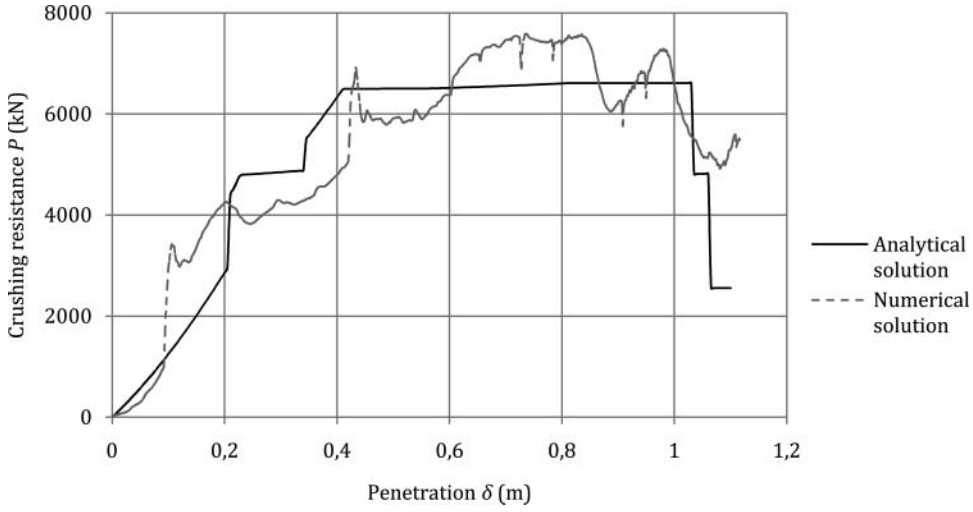

Figure 32. Numerical and analytical resistance curves for gate model 2.3.

8. Conclusion

In this paper, we aim to present a simplified analytical method for estimating the total force acting on a mitre gate when it is collided by a vessel. It is important to bear in mind that our investigations are limited by some hypotheses recalled hereafter:

- Only one leaf of the gate is collided: in this paper, we do not consider a 'centred impact'. This means that the first contact point between the striking vessel and the structure may not be located near the central studs. This last collision scenario is still under investigation.
- The mitre gate is assumed to have single plating; structures with double plating or caissons are not covered in this paper. Moreover, we considered gates with a classical orthogonal stiffening system, like the one depicted in Figure 3.
- The shape of the striking stem is idealised by a parabola. In particular, our methodology does not cover collisions implying barges, for example.

To assess the crashworthiness of the gate, we make the assumption that its behaviour may be divided into two distinct phases. At the beginning, for rather small values of the penetration, the resistance is mainly provided through local crushing of some structural components. During this phase, the region concerned by the impact is localised around the first contact point. Only this zone suffers heavy

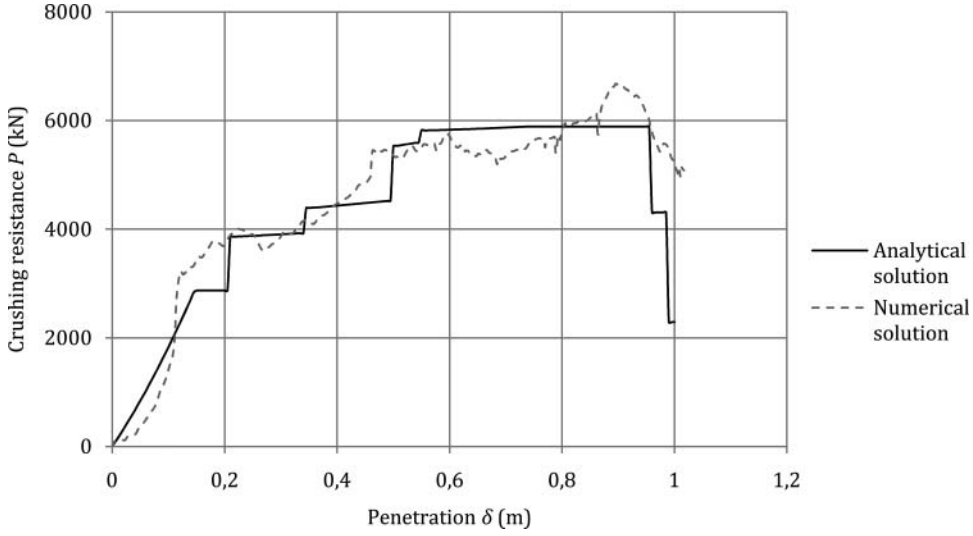

Figure 33. Numerical and analytical resistance curves for gate model 2.4.

deformations; the remaining parts of the gate are still unaffected. To evaluate the resistance for this local deforming mode, the structure is divided into different entities, called super-elements.

For increased values of the penetration, the ship forces the structure to describe an overall bending movement, instead of progressing through local crushing. This second phase is called the global deforming mode. In this case, to assess the resistance, the structure is idealised as a set of independent beams, submitted to a chosen displacement field. These beams have to collaborate because of the action provided by the vertical frames. In this paper, the global mode is investigated considering both elastic and plastic behaviours of the gate. A sliding condition is also introduced to simulate the loss of contact that may occur between the two leafs.

Finally, we propose a comparison between some numerical results and those obtained by the present simplified approach. In most cases, our procedure leads to a quite satisfactory and conservative estimation of the resistance.

The main advantage of our methodology is to give a quick estimation of the ability for a mitre gate to withstand to collisions. Considering a ship with mass M_0 and velocity V_0, the curves depicted in Section 7 are useful to know if such structures are able to absorb a given amount of energy $(M_0 V_0^2/2)$ without suffering excessive damages. It this article, it is not our purpose to detail what are the so-called 'excessive damages' that may affect a mitre gate, because such criteria are most of the time related to the project under consideration. On the contrary, we are much more concerned by developing a simplified mechanical model for these gates. Of course, we have to be conscious that our work is only applicable when pre-designing locks. For more advanced stages of a project, it seems to be unavoidable to use more sophisticated tools, like finite elements analyses.

References

[1] J. Amdahl, *Energy Absorption in Ship-Platform Impact*, PhD. diss., Department of Marine Technology, Norwegian University of Science and Technology, 1983.

[2] L. Buldgen, H. Le Sourne, N. Besnard, and P. Rigo, *Extension of the super-elements method to the analysis of oblique collision between two ships*, Mar. Struct. 29 (2012), pp. 22–57.

[3] L. Buldgen, H. Le Sourne, and P. Rigo, *Simplified analytical method for estimating the resistance of lock gates to ship impacts*, J. Appl. Math. (2012), Article ID 763849, 39 p.

[4] European Committee for Standardization, *Eurocode 3: Design of steel structures – Part 1.5: Plated structural elements, prEN 1993-1-5:2003,* Institut Belge de Normalisation, Brussels, 2003.

[5] International Association of Waterborne Transport Infrastructures, *Innovation in navigation lock design, Report 106,* PIANC, Brussels, 2009.

[6] N. Jones, *Structural Impact*, Cambridge University Press, Cambridge, MA, 1997.

[7] H. Le Sourne, N. Besnard, C. Cheylan, and N. Buannic, *A ship collision analysis program based on upper bound solutions and coupled with a large rotational ship movement analysis tool*, J. Appl. Math. (2012), Article ID 375686, 27 p.

[8] H. Le Sourne, J.C. Rodet, and C. Clanet, *Crashworthiness analysis of a lock gate impacted by two river ships*, Int. J. Crashworthiness 7 (2002), pp. 371–396.

[9] B.C. Simonsen, *Ship grounding on rock – I. Theory*, Mar. Struct. 10 (1998), pp. 519–562.

[10] B.C. Simonsen and H. Ocakli, *Experiments and theory on deck girder crushing*, Thin Wall. Struct. 34 (1999), pp. 195–216.

[11] Y. Ueda and S.M.H. Rashed, *The idealized structural unit method and its application to deep girder structures*, Comput. Struct. 18 (1984), pp. 277–293.

[12] T. Wierzbicki and J. Culbertson-Driscoll, *Crushing damage of web girders under localized static loads*, J. Constr. Steel Res. 33 (1995), pp. 199–235.

[13] S.M. Zhang, *The Mechanics of Ship Collisions*, PhD. diss., Department of Naval Architecture and Offshore Engineering, Technical University of Denmark, 1999.